

Characterization of chromatic dispersion in photonic crystal fibers using scalar modulation instability

G. K. L. Wong, A. Y. H. Chen, S. W. Ha, R. J. Kruhlak,
S. G. Murdoch, R. Leonhardt, and J. D. Harvey

*Department of Physics, University of Auckland, Private Bag 92019,
Auckland, New Zealand*

kwon087@postbox.auckland.ac.nz

N. Y. Joly

*Optoelectronics Group, Department of Physics, University of Bath,
Claverton Down, Bath BA2 7AY, United Kingdom*

Abstract: A simple and accurate method is proposed for characterizing the chromatic dispersion of high air-filling fraction photonic crystal fibers. The method is based upon scalar modulation instability generated by a strong pump wave propagating near the zero-dispersion wavelength. Measuring the modulation instability sideband frequency shifts as a function of wavelength gives a direct measurement of the fiber's chromatic dispersion over a wide wavelength range. To simplify the dispersion calculation we introduce a simple analytical model of the fiber's dispersion, and verify its accuracy via a full numerical simulation. Measurements of the chromatic dispersion of two different types of high air-filling fraction photonic crystal fibers are presented.

© 2005 Optical Society of America

OCIS codes: (060.2270) Fiber characterization; (190.4370) Nonlinear optics, fibers; (190.4380) Nonlinear optics, four-wave mixing.

References and links

1. T. A. Birks, J. C. Knight, and P. St. J. Russell, "Endlessly single-mode photonic crystal fiber," *Opt. Lett.* **22**, 961-963 (1997).
2. J. C. Knight, T. A. Birks, P. St. J. Russell, and J. P. de Sandro, "Properties of photonic crystal fiber and the effective index model," *J. Opt. Soc. Am. A* **15**, 748-752 (1998).
3. A. Ferrando, E. Silvestre, J. J. Miret, P. Andrés, and M. V. Andrés, "Full-vector analysis of a realistic photonic crystal fiber," *Opt. Lett.* **24**, 276-278 (1999).
4. T. M. Monro, D. J. Richardson, N. G. R. Broderick, and P. J. Bennett, "Holey optical fibers: an efficient modal model," *J. Lightwave Technol.* **17**, 1093-1102 (1999).
5. D. Mogilevtsev, T. A. Birks, and P. St. J. Russell, "Localized function method for modeling defect modes in 2-D photonic crystals," *J. Lightwave Technol.* **17**, 2078-2081 (1999).
6. F. Brechet, J. Marcou, D. Pagnoux, and P. Roy, "Complete analysis of the characteristics of propagation into photonic crystal fibers, by the finite element method," *Opt. Fiber Technol.* **6**, 181-191 (2000).
7. M. J. Steel, T. P. White, C. Martijn de Sterke, R. C. McPhedran, and L. C. Botten, "Symmetry and degeneracy in microstructured optical fibers," *Opt. Lett.* **26**, 488-490 (2001).
8. G. E. Town and J. T. Lizier, "Tapered holey fibers for spot-size and numerical-aperture conversion," *Opt. Lett.* **26**, 1042-1044 (2001).
9. M. Qiu, "Analysis of guided modes in photonic crystal fibers using the finite-difference time-domain method," *Microwave Opt. Technol. Lett.* **30**, 327-330 (2001).

10. M. J. Gander, R. McBride, J. D. C. Jones, D. Mogilevtsev, T. A. Birks, J. C. Knight, and P. St. J. Russell, "Experimental measurement of group velocity dispersion in photonic crystal fibre," *Electron. Lett.* **35**, 63-64 (1999).
 11. Q. Ye, C. Xu, X. Liu, W. H. Knox, M. F. Yan, R. S. Windeler, and B. Eggleton, "Dispersion measurement of tapered air-silica microstructure fiber by white-light interferometry," *Appl. Opt.* **41**, 4467-4470 (2002).
 12. C. Mazzali, D. F. Grosz, and H. L. Fragnito, "Simple method for measuring dispersion and non-linear coefficient near the zero-dispersion wavelength of optical fibers," *IEEE Photonics Technol. Lett.* **11**, 251-253 (1999).
 13. T. A. Birks, D. Mogilevtsev, J. C. Knight, and P. St. J. Russell, "Dispersion compensation using single-material fibers," *IEEE Photonics Technol. Lett.* **11**, 674-676 (1999).
 14. J. C. Knight, J. Arriaga, T. A. Birks, A. Ortigosa-Blanch, W. J. Wadsworth, and P. St. J. Russell, "Anomalous dispersion in photonic crystal fiber," *IEEE Photonics Technol. Lett.* **12**, 807-809 (2000).
 15. A. Y. H. Chen, G. K. L. Wong, S. G. Murdoch, R. Leonhardt, J. D. Harvey, J. C. Knight, W. J. Wadsworth, and P. St. J. Russell, "Widely tunable optical parametric generation in a photonic crystal fiber," *Opt. Lett.* **30**, 762-764 (2005).
 16. G. P. Agrawal, *Nonlinear Fiber Optics*, 3rd ed., Optics and Photonics Series (Academic, 2001).
 17. A. Yariv, *Optical Electronics in Modern Communications*, 5th ed. The Oxford Series in Electrical and Computer Engineering (Oxford University Press, 1997).
 18. BeamPROP Version 5.0c (RSoft Design Group, Inc., 2002).
 19. G. K. L. Wong, A. Y. H. Chen, S. G. Murdoch, R. Leonhardt, J. D. Harvey, N. Y. Joly, J. C. Knight, W. J. Wadsworth, and P. St. J. Russell, "Continuous-wave tunable optical parametric generation in a photonic-crystal fiber," *J. Opt. Soc. Am. B* (to be published)
-

1. Introduction

Photonic crystal fibers (PCFs) have recently received much attention in both linear and nonlinear fiber optics because of their unique dispersion properties and high nonlinearity. A highly-nonlinear PCF typically consists of an undoped fused silica core surrounded by an array of microscopic air holes running along its length. The air-silica structure in the cladding exhibits an effective cladding refractive index that is lower than the core's refractive index, making it possible to confine light in the core via index guiding [1,2]. The propagation characteristics of a PCF are governed by the size, number and distribution of the air holes that surround the core. Calculation of the propagation constant, and hence the dispersion, of a PCF typically requires a numerical approach because of the complicated transverse refractive index profile. Many modeling techniques have been developed to study the propagation characteristics of PCFs [3-9]. In principle these allow the dispersion of a PCF to be determined numerically from its refractive index profile which is readily obtainable from a scanning electron microscope (SEM) image of the fiber end. In practice, as we will show in this paper, the small calibration errors in the scale and aspect ratio of such images result in non-negligible errors in the calculated chromatic dispersion.

We propose a new method for measuring the chromatic dispersion of a PCF based on the measurement of the modulation instability (MI) sideband frequency shifts observed when pumping around the fiber's zero-dispersion wavelength. The proposed method provides an accurate measurement of the chromatic dispersion of the PCF over a wide wavelength range, centered around the fiber's zero-dispersion wavelength. In addition PCFs are often birefringent, and this method allows the easy measurement of the chromatic dispersion of both axes - a measurement that can be problematic with standard white light techniques [10,11]. The method is similar to previous techniques used to measure the zero-dispersion wavelength, and dispersion slope, of conventional fibers [12]. The wide sideband tunability possible in a PCF allows us to extend these techniques to make a chromatic dispersion measurement which is accurate over a wide wavelength range. The calculation of the fiber's dispersion from the MI frequency shifts is greatly simplified if a simple and accurate analytical model of the fiber's dispersion is available.

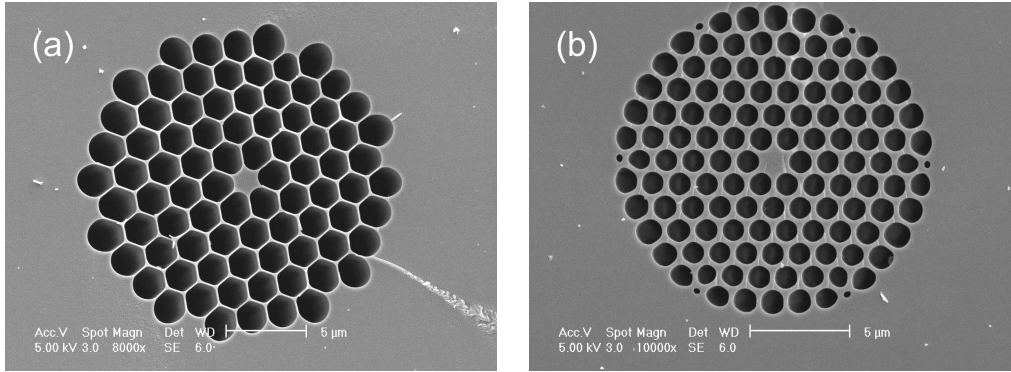


Fig. 1. (a) Scanning electron microscope image of a photonic crystal fiber (fiber A) used in this paper. The light regions are fused silica; the dark regions are air. (b) Scanning electron microscope image of a second photonic crystal fiber (fiber B) used in this paper, where the air-filling fraction is lower.

In the next section we present just such a model.

2. A simple model of the dispersive properties of PCF

The fibers discussed in this paper, in common with many highly-nonlinear PCFs, are not strictly single-mode, and can support several higher-order transverse modes. However experimentally we find that when the launch conditions are optimized for maximum input coupling, over 95% of the light propagates in the fundamental HE₁₁ mode, and so for most practical purposes these fibers can be considered as single-mode. The dispersive characteristics of the fundamental mode of a PCF with a high air-filling fraction in the cladding can be modeled as those of a bare silica strand surrounded by air [13-15]. As the percentage of silica in the cladding increases, the accuracy of this model decreases. We propose an extension to this model that remains accurate for PCFs with lower air-filling fractions. This extension models the PCF as a step-index fiber with a core index set to that of fused silica, and a cladding index set to the mean index of the PCF's cladding. Modeling the material dispersion of fused silica by the standard Sellmeier expansion [16], allows the propagation constant β for the PCF's fundamental mode to be calculated from the standard eigenvalue equation for a step-index fiber [17]. Using the core diameter and the cladding air-filling fraction as free parameters this model can accurately reproduce the dispersive characteristic of high air-filling fraction PCF.

We compare the calculated dispersion of this step-index fiber model to that computed by a full vectorial finite difference beam propagation method for two different high air-filling fraction PCFs [18]. SEM images of the two PCFs are shown in Fig. 1(a) (fiber A) and (b) (fiber B). The numerically calculated group-velocity dispersion β_2 is plotted as a function of wavelength for fiber A and B in Fig. 2(a) and (b) respectively (circles). The model structures used in the numerical simulations were built from the SEM images of the fibers and are shown in the insets to these figures. Superimposed on top of the numerical results are the best-fit β_2 curves calculated from the step-index fiber model. The free parameters in these fits were the effective core diameter and the effective air-filling fraction. For both fibers the agreement between the step-index fiber model and the numerical simulation is better than ± 1 ps²/km over a wavelength range that spans the visible to the near infra-red. This clearly demonstrates that this simple model is capable of accurately reproducing the dispersion of a high air-filling fraction PCF. The small differences between the step-index fiber model and the actual dispersion of the PCF are due to the fact that the step-index fiber model assumes a homogeneous cladding and

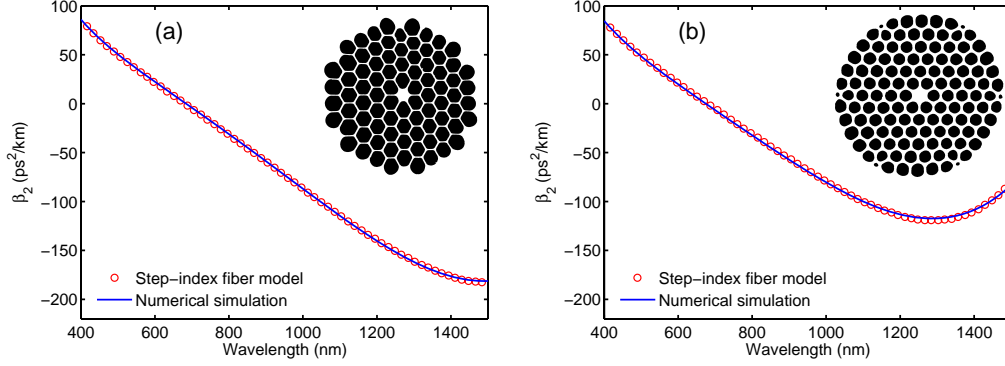


Fig. 2. Group-velocity dispersion as a function of wavelength for (a) fiber A and (b) fiber B. Inset, model structure used in the numerical simulation.

so is unable to exactly reproduce the behaviour of a PCF where the effective cladding index varies as a function of the fraction of the mode propagating in the cladding. The task of calculating the fiber's dispersion from the MI frequency shifts can then be reduced to fitting the predicted MI shifts obtained from the step-index fiber model to the experimentally measured shifts.

3. Modulation instability in PCF

MI originates from the interplay between the nonlinearity and dispersion of the fiber, and results in the generation of sidebands symmetrically placed about the pump frequency ω_p [16]. For an undepleted pump and two weak MI sidebands of the same polarization, the gain spectrum of the sidebands as a function of their frequency detuning Ω from the pump can be written as [15]

$$g(\Omega) = \text{Im} \sqrt{\Delta\beta_L(\Omega) [\Delta\beta_L(\Omega) + 4\gamma P]}, \quad (1)$$

where γ is the fiber's nonlinear interaction coefficient, P is the incident peak power, and $\Delta\beta_L(\Omega)$ is the linear wavevector mismatch between the pump and the sidebands given by

$$\Delta\beta_L(\Omega) = \beta(\omega_p + \Omega) + \beta(\omega_p - \Omega) - 2\beta(\omega_p). \quad (2)$$

The nonlinear interaction coefficient γ is defined as $\gamma = n_2\omega_0/(cA_{\text{eff}})$, where n_2 is the nonlinear refractive index of the fiber and A_{eff} is the effective mode area [16]. The peak of the MI gain is $2\gamma P$, which occurs at a frequency detuning Ω which satisfies the phase-matching condition:

$$\Delta\beta_L(\Omega) + 2\gamma P = 0. \quad (3)$$

Expanding β in a Taylor expansion around the pump wavelength reduces Eq. (3) to

$$\sum_{n=1}^{\infty} \frac{2\beta_{2n}\Omega^{2n}}{(2n)!} + 2\gamma P = 0. \quad (4)$$

Equation (4) clearly shows that the frequency shift of the sidebands is a function of the dispersion of the fiber. For a fiber for which propagation constant β can be accurately approximated by a second-order Taylor expansion, $\Delta\beta_L(\Omega)$ reduces to $\beta_2\Omega^2$, and we recover the standard expression for the gain spectrum of the MI sidebands. This predicts that MI will only occur in the anomalous dispersion regime, with a typically small (few THz) frequency shift. In previous works these small shifts have been used to measure

the zero-dispersion wavelength and the dispersion slope of the fiber under test [12]. The situation is a little different in a PCF; the rapidly varying dispersion around its zero-dispersion wavelength means that higher-order terms on the expansion of β have an important effect on Eq. (4). Consequently the contribution from the higher-order terms can lead to MI sidebands with large frequency shift in the normal dispersion regime. Expanding β even to high order is unsatisfactory as the dispersion curves of these fibers are far from polynomial in shape, so we need to use the exact wavelength dependence of β to calculate $\Delta\beta_L(\Omega)$.

Figure 3 shows the MI sideband phase-matching curve of a high air-filling PCF with an effective core diameter of $1.624\ \mu\text{m}$ and an effective air-filling fraction of 90%. The dispersion of the fiber was calculated from the step-index fiber model, and is shown in the inset to Fig. 3. The pump power was set to be 1 W, and γ to be $100\ \text{W}^{-1}\text{km}^{-1}$, representative values for the experiments discussed in the next section. Figure 3 shows that in the normal dispersion regime, close to the zero-dispersion wavelength, large sideband frequency shifts do indeed occur. These shifts contain information about the dispersion of the fiber over a large wavelength range. Experimentally it is not possible to observe the entire tuning curve of Fig. 3, but rather only a portion of it around the zero-dispersion wavelength. A detailed analysis of MI in a PCF shows that fluctuations in the fiber's core diameter along its length reduce the gain of the sidebands as their frequency shift increases, and therefore limit the observable tuning range [19].

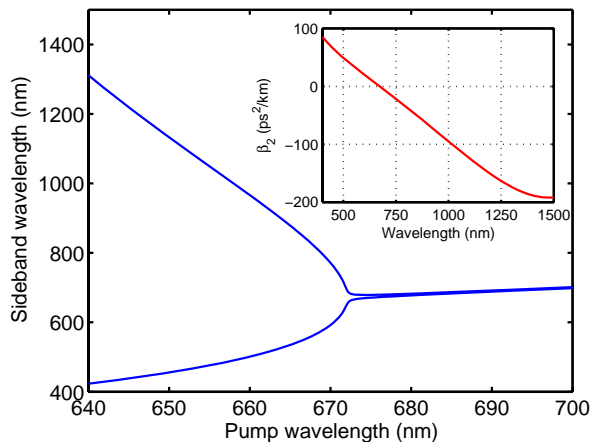


Fig. 3. Modulation instability phase-matching diagram for a photonic crystal fiber with an effective core diameter of $1.624\ \mu\text{m}$ and an effective air-filling fraction of 90%. The pump power was 1 W. Inset, dispersion of the fiber as a function of wavelength.

4. Experimental Results

The pump source used to characterize the dispersive properties of our PCFs is a cavity-dumped tunable DCM-dye laser. An intracavity Lyot filter allows us to tune the wavelength of the laser between 600 and 700 nm. The pulse width of the laser is approximately 13 ns and has a peak power of 6 W. Cavity-dumped pulses from the dye laser were coupled into 60-m lengths of both PCFs with a $60\times$ microscope objective. A half-wave plate was placed in front of the fiber so that the pump could be launched polarized parallel to either the high or low group-index mode as both fibers exhibit significant birefringence ($\Delta n \sim 10^{-4}$). The spectrum at the output of the PCF was recorded using an optical spectrum analyzer. Figure 4 shows the measured MI sideband wavelengths as a function

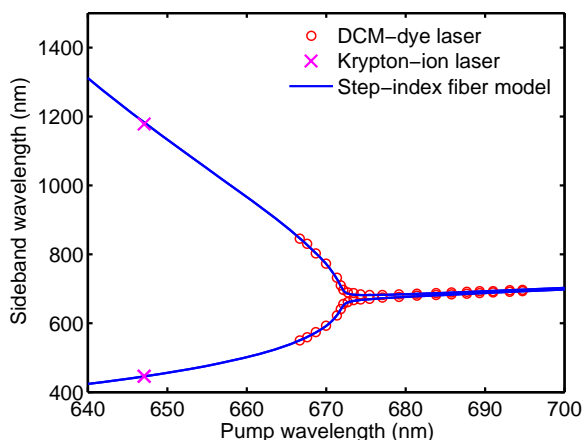


Fig. 4. Experimentally measured sideband wavelengths as a function of pump wavelength for fiber A. The solid curves are the least squares fit to the experimental data (circles), calculated using Eq. (3) based on our step-index fiber model.

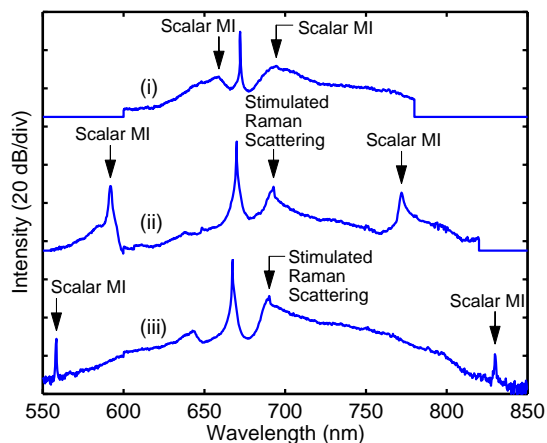


Fig. 5. Optical spectra at the output of fiber A for pump wavelengths (i) 672.2, (ii) 670, and (iii) 667.6 nm (pump polarized to the high group-index mode). The peak power of the pump pulses was 1.5 W.

of pump laser wavelength for fiber A when the pump is polarized parallel to the high group-index mode. The approximate peak power of the pump pulses coupled into the fiber was 1.5 W. Superimposed on top of the experimentally measured shifts (circles) are the best-fit phase-matching curves calculated using Eq. (3) and the step-index fiber model. The free parameters in these fits were the effective core diameter, and the effective air-filling fraction, which were found to be $1.624 \mu\text{m}$, and 90% respectively. In Fig. 5, we plot the experimentally observed spectra at the output of fiber A for pump wavelengths of 667.6, 670, and 672.2 nm. The MI sidebands which we use to measure the fiber's dispersion are clearly visible.

The validity of our predicted tuning curve is confirmed by using a second high power pump source. This laser was a modelocked cavity-dumped krypton-ion laser providing 60-ps pulses at 647.1 nm. These pump pulses were coupled into a 2-m length of fiber A with a peak power of 60 W. When pumping on the high group-index mode we observe sideband wavelengths of 446 and 1178 nm. These additional points are plotted in Fig. 4

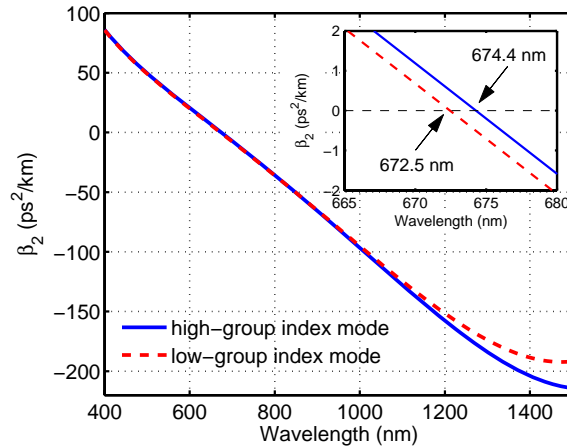


Fig. 6. Measured group-velocity dispersion of fiber A. Inset, close-up of β_2 near the zero-dispersion wavelength

as crosses, and agree almost exactly with the predictions of the step-index fiber model tuning curve (445.4 and 1182.3 nm). This demonstrates that the predicted tuning curve, and hence the dispersion measurement, is accurate over a wavelength range from 400 to 1200 nm. The above measurements were also repeated with the pump polarized parallel to the low group-index mode. In Fig. 6 we plot the dispersion of both the low and high group-index modes of fiber A obtained from the fitted MI tuning curves. The inset to Fig. 6 shows a close up of the fiber's dispersion around the zero-dispersion wavelength. The accuracy of these measurements can be estimated by calculating the change in dispersion necessary to produce a measurable difference between the experimental and the theoretical sideband frequency shifts. At 647 nm, a change of $\pm 1\%$ in the dispersion would produce approximately ± 5 THz shift in the calculated sideband frequency. As our calculated sideband frequency shifts agree to within 1.5 THz with the experimental sideband frequency shifts, the accuracy of the dispersion measurement is well within $\pm 1\%$, and therefore the accuracy of the zero-dispersion wavelength can be calculated to be ± 0.3 nm. We note that this accuracy is much better than can be obtained from a numerical calculation of the dispersion which uses a measurement of the fiber's refractive index profile from an SEM image. The scale error in the SEM images shown in Fig. 1(a) and (b) is 2%, which results in an error of ± 4 nm in the predicted zero-dispersion wavelength. Although the MI sideband frequency shift depends on the nonlinear term $2\gamma P$ close to the zero-dispersion wavelength, a small change in the nonlinear interaction coefficient γ would not produce a measurable error in the dispersion and the zero-dispersion wavelength. We find a change of $\pm 5\%$ in γ only produces approximately $\pm 0.1\%$ difference in the dispersion and consequently a ± 0.05 nm shift in the zero-dispersion wavelength. This is because the MI sidebands with large frequency shift contain information about the dispersion over a large wavelength range including the zero-dispersion wavelength, and the frequency shifts of these sidebands are dominated by the linear phase-matching condition.

We repeated the above measurements for both the low and high group-index modes of fiber B. The measured sideband wavelengths for the high group-index mode are shown in Fig. 7. Again excellent agreement is found between the measured and fitted sideband frequency shifts. The effective core diameter and the effective air-filling fraction were found to be $1.554 \mu\text{m}$ and 0.78, respectively. This allows us to calculate the dispersion of fiber B using the same procedure used for fiber A. In Fig. 8 the measured dispersion

of the fiber B for both the high and low group-index modes is shown. The uncertainty in this measurement is the same as that for fiber A. A comparison of the measured dispersion curves of fibers A and B (Fig. 6 and 8) shows that while both have very similar zero-dispersion wavelengths, the lower air-filling fraction of fiber B results in a flatter dispersion curve.

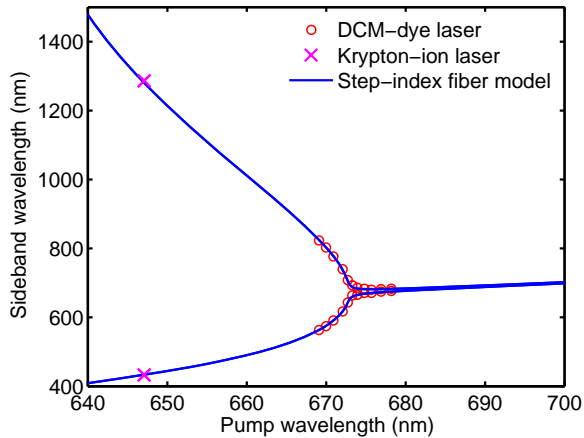


Fig. 7. Experimentally measured sideband wavelengths as a function of pump wavelength for fiber B. The solid curves are the least squares fit to the experimental data (circles), calculated using Eq. (3) based on our step-index fiber model.

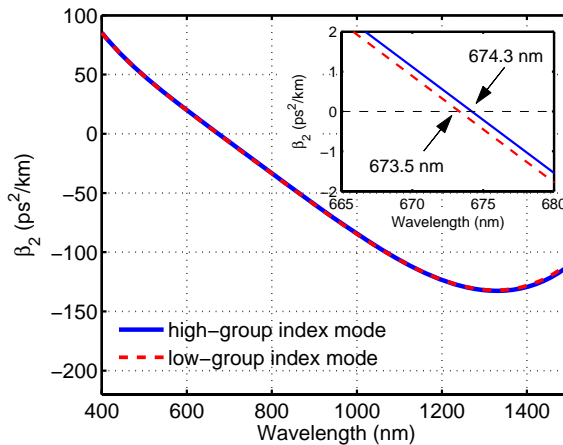


Fig. 8. Measured group-velocity dispersion of fiber B. Inset, close-up of β_2 near the zero-dispersion wavelength

5. Conclusion

In conclusion, we have presented a simple and accurate method for determining the chromatic dispersion of high air-filling fraction highly-nonlinear PCFs, based on the measurement of MI sideband frequency shifts in the normal dispersion regime. We demonstrate that the dispersion of high air-filling fraction PCFs can be well approximated as the dispersion of a step-index fiber with an effective core diameter equal to that of the central silica rod, and a cladding index approximated to the mean refractive index of the cladding. This allows us to evaluate the chromatic dispersion analytically without

the need for computationally intensive numerical simulation. By using a tunable laser source with a limited tuning range (~ 10 nm) around the zero-dispersion wavelength of the fiber, it was possible to characterize the dispersion accurately from 400 to 1200 nm for both optical axes of the fiber. The method is particularly applicable to the characterization of large air-filling fraction PCF. We have performed full vectorial numerical simulations for fibers with a range of air-filling fractions (10%-90%) and found that the step-index fiber model is very accurate in all cases. This implies that the method proposed here is applicable to any such PCF provided a suitable tunable pump laser is available. The method is also applicable to the characterization of conventional optical fibers provided that their dispersion curves result in MI sidebands with large frequency shift.